*Journal of Structural Geology*, Vol. 13, No. 3, pp. 337 to 347, 1991
Printed in Great Britain

0191-8141/91 $03.00+0.00


# Significance of low symmetry fabrics in magmatic rocks

ANGEL FERNANDEZ

Université de Limoges, Laboratoire de Géologie Régionale et Appliquée, 123 Av. Albert Thomas 87060 Limoges Cédex, France, and U.R.A., No. 10 CNRS, Clermont-Fd, France

and

DIDIER LAPORTE*

Université de Saint-Etienne, Laboratoire de Géologie, 23 rue du Dr Paul Michelon, 42023 Saint-Etienne Cédex 2, France

(*Received* 8 *February* 1989; *accepted in revised form* 28 *June* 1990)

**Abstract**—The significance of low symmetry fabrics (monoclinic and triclinic) in magmatic rocks is studied using theoretical models describing the motion of rigid markers embedded in a slowly deforming ductile matrix. In agreement with Curie's Symmetry Principle, the development of these fabrics requires a non-coaxial strain-path. Simulations of monoclinic fabrics indicate that their characteristics depend on: (a) the strain regime and the amount of strain, and (b) the morphological composition of the population of rigid markers.

Natural monoclinic fabrics contain precious information about the strain regime they result from: type of the non-coaxial strain-path involved (simple shear, non-coaxial flattening, etc.), orientation of its axes and sense of shear. The magnitude of the finite strain may eventually be estimated provided that the shape of the markers is precisely known.

## INTRODUCTION

THE existence of low symmetry fabrics in magmatic rocks has long been recognized (Sander 1948). According to this author, most megascopic magmatic structures are monoclinic: indeed they display a unique symmetry plane normal to a rotation axis (*B*-axis). Examples are: (a) lava flows with asymmetric profiles showing superficial rolls, folds and vortices, and (b) roll-folds around rotated inclusions.

Instead of considering such large-scale structures, we shall discuss here the case of the pervasive preferred dimensional orientation (P.D.O.) often displayed by magmatic rocks. In this paper, the term fabric refers to the bulk P.D.O. of a given sample; in the same sample, a specific P.D.O. or 'subfabric' may be defined for each different mineral or for different families of a given mineral. A precise knowledge of the fabric symmetry results from the statistical analysis of P.D.O. and the construction of pole-figures (see for instance Weiss & Wenk 1985). Igneous rocks present evidence of a large variety of fabrics and corresponding symmetries. We discuss here the case of low symmetry fabrics.

According to Curie's Symmetry Principle (Curie 1894, Nicolle 1950, Paterson & Weiss 1961), a close relationship is expected between low symmetry fabrics and non-coaxial strain regimes. However, symmetry considerations alone cannot account for the diversity of low symmetry fabrics—especially monoclinic fabrics—encountered in igneous rocks (Fig. 1). In order to explain this diversity, magmatic fabrics have been modelled using the equations of motion of rigid ellipsoids suspended in a slowly deforming ductile matrix (Jeffery 1922). The characteristics of the resulting fabrics depend on: (a) the strain regime and the amount of strain, and (b) the morphological composition of the population of rigid markers. In this paper we present simulations of monoclinic fabrics resulting from different non-coaxial strain histories: (a) simple shear, (b)

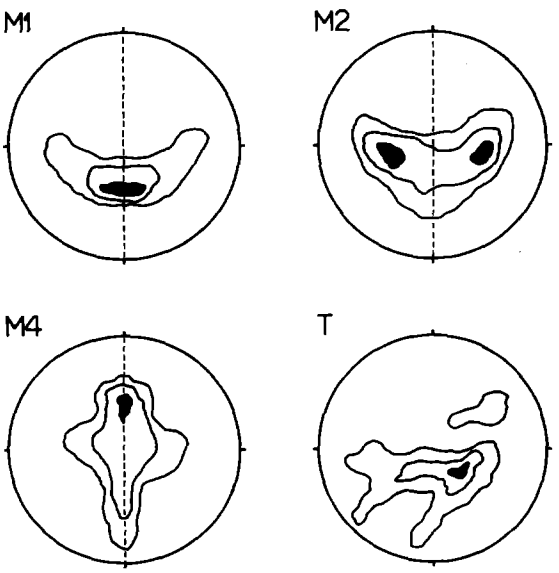


Fig. 1. Main kinds of low symmetry fabrics encountered in porphyroid granitoids (120 measures of (010) planes of K-feldspar megacrysts; modified from Fernandez 1982). M1, M2 and M4 are three common types of monoclinic pole-figures; dashed line: symmetry plane. T is a triclinic pole-figure.

*Present address: Université Blaise Pascal, CNRS, U.R.A. No. 10, 5 rue Kessler, 63038 Clermont-Fd Cedex, France.

non-coaxial flattening and (c) axial flattening followed by simple shear.

The comparison of natural and simulated fabrics places severe constraints on the geometry of the flow regime governing the preferred orientation development. Ultimately, the magnitude of the finite strain may be estimated when the actual shape of the rigid markers is known.

## FABRIC SYMMETRY AND STRAIN REGIME

### *Strain regimes*

Consider a set of orthogonal Cartesian axes $X_i'$ ($i = 1,2,3$) fixed in orientation. In this reference frame, the flow of the deforming magma may be specified by the velocity gradient tensor $T'$ (Freeman 1985). If the nine components:

$$T_{ij}' = \mathrm{d}v_i'/\mathrm{d}x_j' \qquad (1)$$

of $T'$ are constant with time, a steady flow or 'strain regime' is defined. In the following, we shall deal with isovolumetric strain (a condition satisfied by the relation $T_{11}' + T_{22}' + T_{33}' = 0$). The strain regimes we consider below are depicted in Fig. 2 and their main characteristics are summarized in Table 1.

General non-coaxial strain regimes may be described as combinations of a simple shear and a coaxial component (Ramberg 1975). They have a monoclinic symmetry when the unique symmetry plane of the shear component (M for 'mirror' in Fig. 2) coincides with one of the symmetry planes of the coaxial component; otherwise, they have a triclinic symmetry. Similarly, the symmetry of polyphased strain histories is defined by the symmetry elements common to the successive strain regimes.

### *Curie's Principle and the origin of low symmetry fabrics*

Curie's Principle governs the symmetry of causes and effects in physical phenomena and may be expressed as follows (Paterson & Weiss 1961): "*Whatever the nature of the factors contributing to a deformation may be, the symmetry that is common to them cannot be higher than the symmetry of the deformed fabric, and symmetry elements absent in this fabric must be absent in at least one of the contributing factors*".

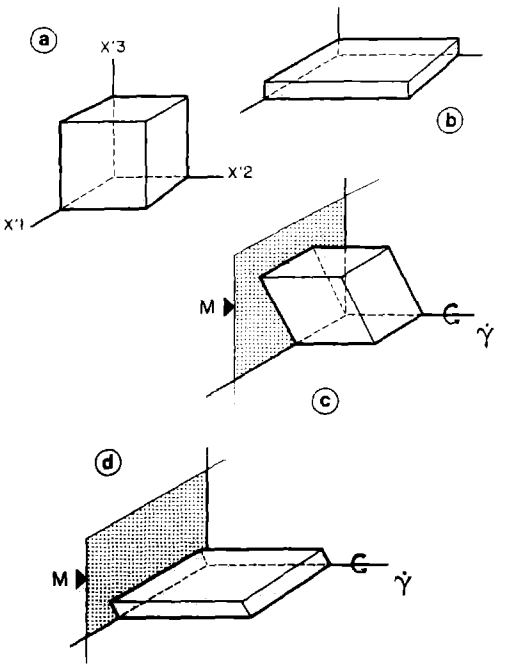


Fig. 2. (a) Transformation of a unit cube during: (b) axial flattening; (c) simple shear; and (d) non-coaxial flattening. M is the symmetry plane of the non-coaxial strain regimes.

Preferred orientations displayed by magmatic rocks usually result from the rigid rotation of phenocrysts suspended in their slowly deforming ductile matrix, whatever the meaning of this deformation is (magmatic emplacement, regional stress field, etc., Fernandez 1984). In this context the contributing factors to the development of the final fabric are: (a) the shape of the crystals (or "markers"), (b) their initial distribution and (c) the deformation history (or 'magmatic flow'). Assuming the initial distribution to be isotropic, Curie's Principle implies that low symmetry P.D.O. are developed in response to strain regimes—or polyphased strain histories—with a non-coaxial component. An additional requirement for the development of low symmetry P.D.O. concerns the shape and/or the distribution of shapes of the markers; in the case of ellipsoidal markers, it is shown below that fabrics developed in response to simple shear are monoclinic when one of the following conditions is satisfied:

(i) the markers are spheroids with various axial ratios $n$ or shape coefficients $K = (n^2 - 1)/(n^2 + 1)$; $n$ is defined as the ratio of the length $2a$ of the revolution axis

Table 1. Strain regimes and their symmetry

| Strain regime* | Tensor | Symmetry |
|---|---|---|
| Axial flattening (c.) | $T_{11}' = T_{22}' > 0$<br>$T_{33}' = -2T_{11}'$ | axial |
| Simple shear (n.c.) | $T_{13}' = \dot{\gamma}\ (\neq 0)$ | monoclinic |
| Non-coaxial flattening (n.c.) | $T_{11}' = T_{22}' > 0$; $T_{33}' = -2T_{11}'$<br>$T_{13}' = \dot{\gamma}\ (\neq 0)$ | monoclinic |

*c., coaxial; n.c., non-coaxial. Only the non-zero components of the velocity gradient tensor are given.

divided by the length $2b = 2c$ of the two other principal axes;

(ii) the markers are triaxial ellipsoids.

## BASIC EQUATIONS OF MOTION FOR RIGID PARTICLES

Consider a triaxial ellipsoid of neutral buoyancy isolated in a deforming fluid and let $X_1$, $X_2$, $X_3$ be three orthogonal axes coincident with the principal axes $2a$, $2b$, $2c$ of the ellipsoidal particle and moving with them. The velocity gradient tensor $T$, referred to this co-ordinate system, may be divided into its symmetric part $E$ and antisymmetric part $R$. The equations of motion referred to the rotating co-ordinate system are (Jeffery 1922, Willis 1977):

$$\begin{aligned}\omega_1 &= [(b^2 - c^2)/(b^2 + c^2)] \times E_{23} + R_{32}\\ \omega_2 &= [(c^2 - a^2)/(c^2 + a^2)] \times E_{31} + R_{13}\\ \omega_3 &= [(a^2 - b^2)/(a^2 + b^2)] \times E_{12} + R_{21},\end{aligned} \tag{2}$$

where $\omega_i$ are the angular velocities of the ellipsoid around its own axes $X_i$. These equations describe the motion of an isolated particle; however, if the volume concentration of spheroids is small enough to preclude interactions between rotating grains, then the development of preferred orientation in multi-particle systems may be investigated. In the special case of spheroids (axial ellipsoids), the analytical solutions of equations (2) are known for simple flow regimes (simple shear, Jeffery 1922; pure shear, Gay 1968; axial flattening, Debat *et al.* 1975, Tullis 1976). For complex flows such as general non-coaxial strain regimes, the analytical solutions of equations (2) are unknown. In the case of an isotropic initial distribution of rigid particles, Willis (1977, p. 889) showed that, whatever the strain regime is, the resulting fabric for axial markers of a given shape $K$ may be described by an ellipsoid, namely the fabric ellipsoid; for an isovolumetric strain, the density $D$ of grain axes lying in a given direction, relative to a uniform distribution of axes orientations, is:

$$D = l^3, \tag{3}$$

where $l$ is the radius of the fabric ellipsoid in this direction. For a strain regime defined by its velocity gradient tensor $T'$ and acting over the specified time $t$, the fabric ellipsoid coincides with the strain ellipsoid for the hypothetical strain regime $T^*$ acting over the same time $t$ (Willis 1977):

$$T^*_{ij} = (K \times E'_{ij}) + R'_{ij}, \tag{4}$$

$E'$ and $R'$ being the symmetric and antisymmetric parts of $T'$. Willis's model may be extended to heterogeneous populations of axial markers by dividing them into quasi-homogeneous subpopulations made of markers with close values of $K$. Subfabric ellipsoids may then be defined by assigning to each subpopulation an average value of $K$. The bulk density $D$ in a given direction is (Fernandez 1984):

$$D = \Sigma^k f_k \times l_k^3, \tag{5}$$

where $f_k$ is the proportion of subpopulation $k$ and $l_k$ is the radius of the subfabric ellipsoid $k$ in this direction.

In the following, Willis's model has been used to compute the preferred orientation of axial markers in non-coaxial strain regimes with monoclinic symmetry. Fabric ellipsoids are defined by the orientation and the value of their principal axes $\Lambda_1$, $\Lambda_2$, $\Lambda_3$ (with $\Lambda_1 > \Lambda_2 > \Lambda_3$). They are plotted in a diagram $(\Lambda_2/\Lambda_3)^{1/2}$ vs $(\Lambda_1/\Lambda_3)^{1/2}$, equivalent to Flinn's diagram for the strain ellipsoids (Flinn 1962). For heterogeneous populations, fabrics are illustrated by pole-figures (lower-hemisphere Schmidt projection). In these projections, the simple shear component of non-coaxial strain regimes (Figs. 2c & d) is orientated as follows: (a) the $X'_2$ axis is horizontal, E–W, and (b) the $X'_1$–$X'_3$ plane is vertical, N–S. In order to visualize asymmetry, density profiles in the plane $X'_1 - X'_3$ are displayed.

## FABRIC DEVELOPMENT IN SIMPLE SHEAR REGIME

### *Motion of an isolated spheroid*

The motion of rigid axial particles in a viscous fluid undergoing simple shear is described by the following equations (Jeffery 1922, Reed & Tryggvason 1974, Blanchard *et al.* 1979):

$$\begin{aligned}\tan\phi_f &= n \times \tan[(n \times \gamma)/(n^2 + 1) + \arctan((\tan\phi_i)/n)]\\ \tan^2\theta_f &= \tan^2\theta_i \times [(n^2 \times \cos^2\phi_i\\ &\quad + \sin^2\phi_i)/(n^2 \times \cos^2\phi_f + \sin^2\phi_f)].\end{aligned} \tag{6}$$

Here $n$ is the axial ratio of the particle and $\gamma$ is the amount of shear; $\phi$ and $\theta$ (radians) define the orientation of the revolution axis of the particle (Fig. 3), and subscripts i and f refer to the initial and final angles, respectively. Equations (6) indicate that the motion of an axial rigid particle in a simple shear regime is periodic; the amount of shear necessary to complete a

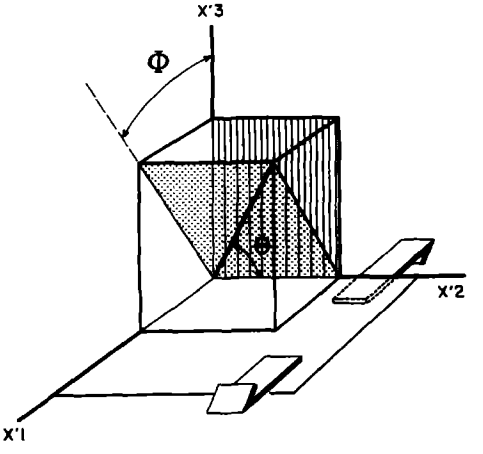


Fig. 3. Azimuth $\phi$ and plunge $\theta$ of the revolution axis (thick line) of an axial marker in simple shear regime.

rotation of the particle is (Willis 1977, Fernandez *et al.* 1983, Fernandez 1984):

$$\gamma_{T,M} = (2\pi \times (n^2 + 1))/n = 4\pi/(1 - K^2)^{1/2}. \quad (7)$$

In the course of a rotation, the revolution axis describes a closed orbit about $X_2'$. When $\gamma = \gamma_{T,M}$, the particle returns to its original orientation ($\phi_i = \phi_f$ and $\theta_i = \theta_f$). Perfectly linear or planar rigid markers ($K = 1$ and $K = -1$, respectively) have a non-periodic motion and remain fixed when they reach the shear plane.

*Homogeneous population of spheroids*

For a given value of $K$, the shape and the orientation of the fabric ellipsoid changes during progressive simple shear. According to Curie's Principle, one of the symmetry planes of this ellipsoid must coincide with the symmetry plane $X_1' - X_3'$ of the simple shear. Because simple shear is a plane strain, the intermediate axis of the fabric ellipsoid is parallel to $X_2'$ and is unity. Consequently the planes $X_1' - X_3'$ and $\Lambda_1 - \Lambda_3$ coincide. The orientation of $\Lambda_1$ in the plane $X_1' - X_3'$ is specified by the angle $\alpha$ (Fig. 4). During progressive simple shear, the following evolutions are predicted (Fig. 5):

(i) $\Lambda_1$ axis rotates around $X_2'$ with a period (Fernandez *et al.* 1983):

$$\gamma_{T,F} = 2\pi/(1 - K^2)^{1/2}. \quad (8)$$

The initial orientation for an infinitely small shear strain is $\alpha = -45°$; when $\gamma = \gamma_c = \pi/(1 - K^2)^{1/2}$, $\alpha = 0°$, the foliation and the lineation ($\Lambda_1 - \Lambda_2$ and $\Lambda_1$ for linear particles; $\Lambda_2 - \Lambda_3$ and $\Lambda_3$ for planar particles) transpose the shear plane and the shear direction, respectively, $\gamma_c$ being referred to as the critical shear;

(ii) $\Lambda_1$ reaches a maximum value when the shear plane and the shear direction are transposed ($\gamma = \gamma_c$; Fig. 5). Then $\Lambda_1$ decreases and for $\gamma = \gamma_{T,F}$, the initial isotropic fabric is restored. This disorganization effect has been reproduced experimentally by Fernandez *et al.* (1983).

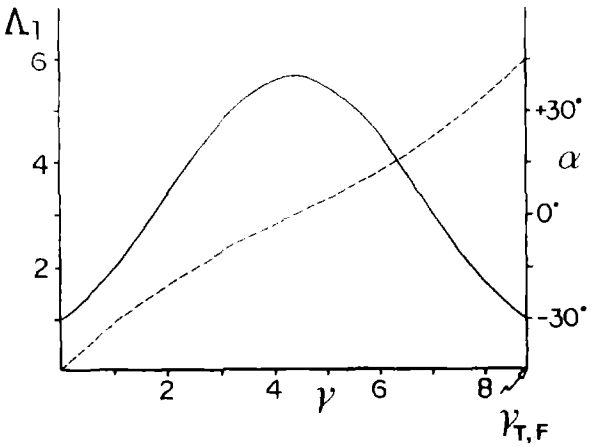


Fig. 5. Evolution of the value (full line) and orientation (dashed line) of the long axis $\Lambda_1$ of the fabric ellipsoid during simple shear; axial markers with $K = -0.7$.

*Heterogeneous population of spheroids: development of monoclinic fabrics*

The evolution of the fabric ellipsoid depends on the value of $K$: (a) the period $\gamma_{T,F}$ increases with the anisometry of the markers (that is with abs($K$), the absolute value of $K$; see equation 8) and (b) the maximum value of $\Lambda_1$, for $\gamma = \gamma_c$, increases with abs($K$). The first relationship is of paramount importance in the understanding of monoclinic fabrics. Consider the case of a heterogeneous population divided into several quasi-homogeneous subpopulations. For a given amount of shear, the subfabric ellipsoids have different orientations of their $\Lambda_1$ axes depending on the shape coefficient $K$, as illustrated in Fig. 6. Therefore their symmetry planes $\Lambda_1 - \Lambda_2$ (and also $\Lambda_3 - \Lambda_2$) do not coincide and the unique symmetry plane of the bulk fabric is the common plane $\Lambda_1 - \Lambda_3$ of the subfabric ellipsoids (Fernandez 1982). We conclude that simple shear acting upon heterogeneous populations of axial markers produces monoclinic fabrics with a symmetry plane coinciding with the deformation plane $X_1' - X_3'$.

A simulation of monoclinic fabric associated with simple shear is presented in Fig. 7 (Fernandez 1984). As

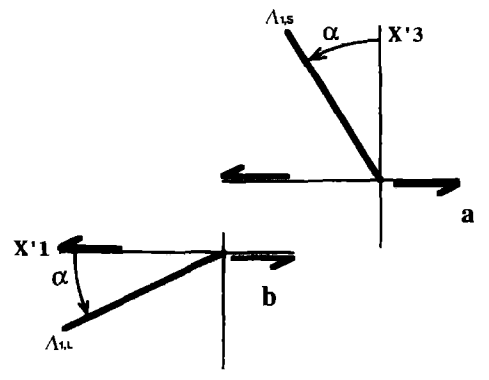


Fig. 4. Orientation of the axis $\Lambda_1$ of the fabric ellipsoid for oblate spheroids (a: $\Lambda_{1,S}$; $\alpha$ referred to axis $X_3'$) and for prolate spheroids (b: $\Lambda_{1,L}$; $\alpha$ referred to axis $X_1'$).

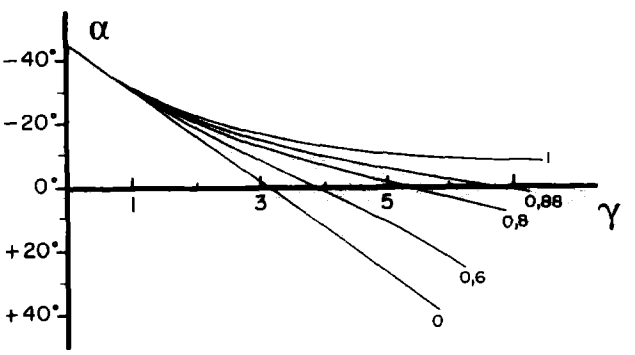


Fig. 6. Family of curves giving the orientation of the fabric ellipsoid (angle $\alpha$) as a function of $\gamma$ for different shape coefficients $K$ (from Fernandez *et al.* 1983).

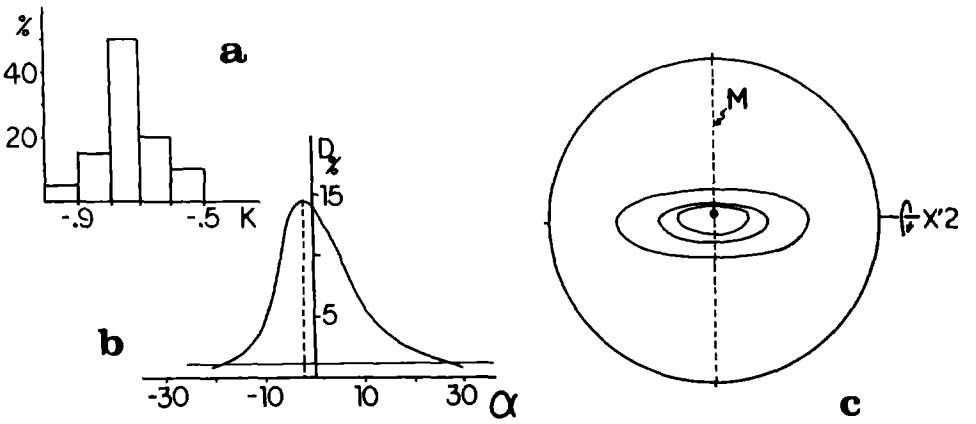


Fig. 7. Monoclinic fabric resulting from a simple shear ($\gamma = 5$) acting upon a heterogeneous population of axial markers; (a) distribution of the shape of the markers; (b) density profile along the symmetry plane of the fabric; and (c) monoclinic pole-figure.

expected, the density profile in the plane $X'_1 - X'_3$ (Fig. 7b) is asymmetric. The density of P.D.O. in the $X'_2$ direction is about unity (Fig. 7c); this may be predicted because simple shear is a plane strain. The resulting fabric compares with the type M1 of monoclinic fabrics listed in Fig. 1.

*Criteria to deduce the sense of shear*

The sense of shear may be inferred from the angular relationships between subfabrics corresponding to different minerals of a rock, for instance biotite and K-feldspar in granitoids (alternatively subfabrics corresponding to different families of the same mineral). Let us consider that biotites and K-feldspar megacrysts compose two quasi-homogeneous populations of oblate spheroids, biotites being more oblate than K-feldspars. In such a system, simple shear leads to the development of a heteroaxial bulk fabric, biotite and K-feldspar subfabrics displaying different orientations (Fig. 8a). Indeed the K-feldspar foliation plane ($S_{Kf}$ in Fig. 8a) which corresponds to the plane $\Lambda_2 - \Lambda_3$ of the subfabric ellipsoid, rotates faster (that is with a smaller period $\gamma_{T,F}$; see equation 8) than the biotite foliation plane ($S_{bt}$ in Fig. 8a). Accordingly, as it is depicted in the right-hand sketch of Fig. 8(a), the sense of rotation in the $X'_1 - X'_3$ plane is from the biotite foliation plane to the K-feldspar foliation plane. This criterion may be extended to monoclinic pole-figures because the density maximum of these diagrams is expected to be defined by the most anisometric markers (this point is illustrated below in the case of non-coaxial flattening). Accordingly, the sense of rotation in the symmetry plane of the pole-figure is from the density maximum (corresponding to highly anisometric markers) to the low density flank of the asymmetric profile (corresponding to markers with low anisometry) (Fig. 8b).

The criteria discussed above are valid only if all the subfabrics involved are still in their first cycle of evolution (that is if $\gamma < 2\pi/(1 - K^2_{min})^{1/2}$, $K_{min}$ being the shape coefficient of the least anisometric markers of the studied population). The reader is referred to Blumenfeld & Bouchez (1988) for a comprehensive review of shear criteria in granites and migmatites.

*Simple shear and triaxial ellipsoids*

Using a numerical approach, Freeman (1985) computed the motion of triaxial ellipsoids in simple shear regime and showed that the orbits the markers describe about $X'_2$ are not closed (i.e. when $\phi_f = \phi_i$, $\theta_f \neq \theta_i$). For multi-particle systems, an insight in the fabric symmetry is offered by considering the case of markers having one of their symmetry planes coincident with $X'_1 - X'_3$. If we consider the density of orientation of the long axis of prolate spheroids (with axes $2a > 2b > 2c$) in the $X'_1 - X'_3$ profile, two different behaviours are predicted depending on which particle axis coincides with $X'_2$:

(i) if $X_3$ coincides with $X'_2$, the motion of the long axis is described by the equation (Willis 1977):

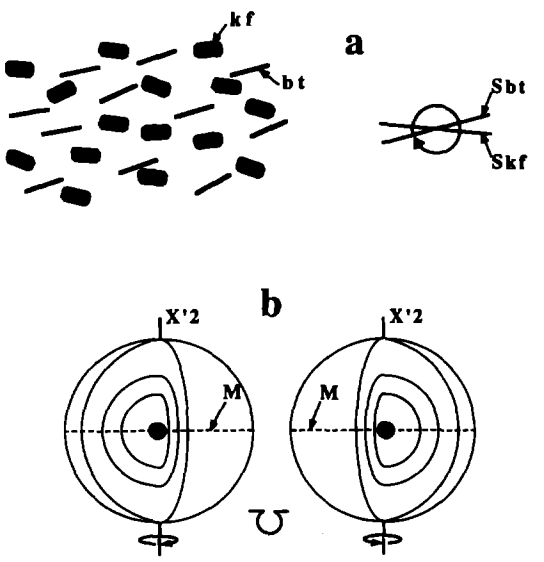


Fig. 8. Criteria to deduce the sense of shear: (a) heteroaxial biotite (bt) and K-feldspar (kf) subfabrics resulting from simple shear (the section coincides with the plane $X'_1 - X'_3$ of the deformation); the sense of rotation is from the biotite foliation plane $S_{bt}$ to the K-feldspar foliation plane $S_{kf}$; (b) sense of shear deduced from the polarity of monoclinic pole-figures (see text for further explanations).

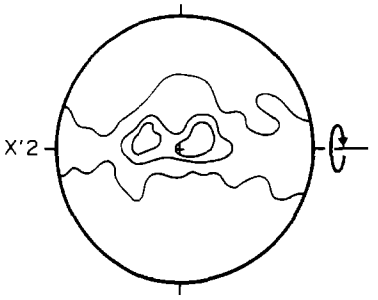


Fig. 9. Simulated fabric resulting from a simple shear ($\gamma = 3$) acting upon a homogeneous population of triaxial markers ($a/b = b/c = 1/3$); the shear plane is horizontal and the sense of shear is indicated by the arrow. The motion of the markers defining an initial isotropic distribution has been computed by numerical treatment; the density contours describe the final distribution of short axes (from Fernandez 1984). Contours: 1, 2.5 and 4%.

$$\omega_3 = \mathrm{d}\phi/\mathrm{d}t = 0.5 \times \dot{\gamma} \times (1 + K_3 \times \cos 2\phi), \quad (9)$$

with $K_3 = (a^2 - b^2)/(a^2 + b^2)$; the corresponding period of rotation is (Fernandez *et al.* 1983):

$$\gamma_{T,M} = 4\pi/(1 - K_3^2)^{1/2}; \quad (10)$$

(ii) if $X_2$ coincides with $X_2'$, the following equations can be written:

$$\omega_2 = \mathrm{d}\phi/\mathrm{d}t = 0.5 \times \dot{\gamma} \times (1 + K_2 \times \cos 2\phi) \quad (11)$$

$$\gamma_{T,M} = 4\pi/(1 - K_2^2)^{1/2}, \quad (12)$$

with $K_2 = (a^2 - c^2)/(a^2 + c^2)$.

For a given amount of shear, the two populations of particles will develop density maxima with different orientations, contributing to the development of an asymmetric density profile. A fabric simulated for triaxial ellipsoids in simple shear regime is presented in Fig. 9 (Fernandez 1984). Its monoclinic symmetry is not well-defined, perhaps because of the low amount of shear ($\gamma = 3$). However this two-maxima diagram is similar to the monoclinic fabric M2 displayed in Fig. 1.

## RELATIONSHIPS BETWEEN THE GEOMETRY OF NON-COAXIAL STRAIN REGIMES AND THE SHAPE OF THE RESULTING MONOCLINIC FABRICS

According to Curie's Principle, the knowledge of fabric symmetry constrains the strain regime symmetry. For a specific kind of fabric symmetry, additional constraints result from the geometry of the pole-figures. This will be demonstrated for monoclinic fabrics by considering the special case of axial markers.

As concluded above, fabrics simulated for simple shear acting upon heterogeneous populations of axial markers (Fig. 7c) compare with type M1 of natural monoclinic fabrics (Fig. 1). Other types of monoclinic P.D.O. have been encountered in igneous rocks, such as the tadpole-shaped M4 diagrams of Fig. 1. By applying the same reasoning as for simple shear and M1 pole-figures, we may conclude that the plane M coincides with the unique symmetry plane of a non-coaxial strain regime. The $X_2'$ direction normal to M cannot be a non-deformation direction because density of orientation along $X_2'$ is less than unity (Fig. 1). For M4 diagrams defined by polar projection of planar elements, $X_2'$ corresponds to an extension direction. Thus, development of tadpole-shaped monoclinic fabrics for planar markers implies the combination of a simple shear component and a coaxial component satisfying the two conditions: (a) the $X_2'$ axis of simple shear corresponds to an extension direction of the coaxial component and (b) the bulk symmetry is monoclinic. There are an infinite number of such combinations; two examples are studied below because they lead to contrasting geological implications:

(i) *non-coaxial flattening*; the corresponding flow geometry is illustrated in Fig. 2(d); for the sake of simplicity, we shall consider the case of coincident shear plane and flattening plane; however, the results presented below (specially those concerning the development of M4 pole-figures) may be extended to more general monoclinic non-coaxial flattenings (Laporte 1987);

(ii) *axial flattening followed by simple shear (polyphased history)*.

### *Fabric development in non-coaxial flattening regimes*

The investigated regime is defined by the velocity gradient tensor:

$$T' = \begin{vmatrix} 0.085 & 0 & \dot{\gamma} \\ 0 & 0.085 & 0 \\ 0 & 0 & -0.17 \end{vmatrix}.$$

Detailed results are presented below for $\dot{\gamma} = 0.7$; variations of $\dot{\gamma}/T_{22}'$ are briefly considered because this ratio envisions the relative importance of simple shear and axial flattening in the non-coaxial regime.

*Case of a homogeneous population*. During the course of a non-coaxial flattening regime, the shape and the orientation of the fabric ellipsoid evolve in a cyclic way. Figure 10 illustrates these evolutions for a population

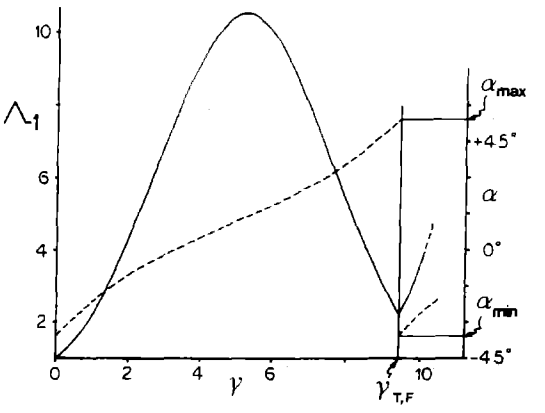


Fig. 10. Evolution of the value (full line) and orientation (dashed line) of the long axis $\Lambda_1$ of the fabric ellipsoid during non-coaxial flattening; axial markers with $K = -0.7$ (see text for further explanations).

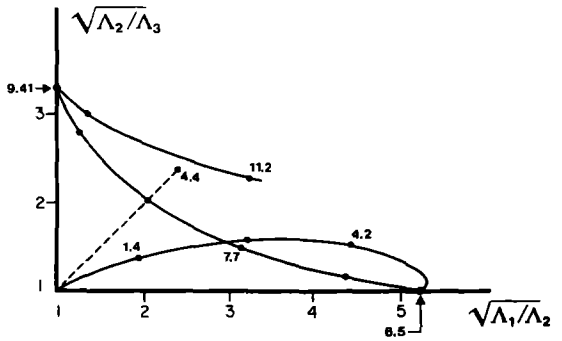


Fig. 11. Evolution of the shape of the fabric ellipsoid during non-coaxial flattening (full line); comparison with simple shear regime (dashed line): numbers indicate the amount of shear ($\dot{\gamma} \times t$).

made of planar particles with $K = -0.7$. The amount of strain is specified by the parameter $\gamma = \dot{\gamma} \times t$.

(i) The variations of $\Lambda_1$ are cyclic but non-periodic (Fig. 10): indeed the successive maxima of the $\Lambda_1 - \gamma$ curve increase and the initial isotropic fabric is not restored at the end of each cycle. The duration of one cycle is $\gamma_{T,F} = 9.41$ (the analytical expression is unknown).

(ii) The orientation of the fabric ellipsoid is fully specified by the angle $\alpha$ of $\Lambda_1$ axis in the plane $X'_1 - X'_3$ of the simple shear component (see Fig. 4). The curve $\alpha - \gamma$ is periodic with a period $\gamma_{T,F} = 9.41$ (Fig. 10); its two boundaries $\alpha_{min} = 36°$ and $\alpha_{max} = +54°$ differ from the equivalent boundaries $-45°$ and $+45°$ observed in simple shear regime (Fig. 5).

(iii) The shape variations of the fabric ellipsoid are displayed in Fig. 11: all kinds of ellipsoids are expected in a non-coaxial flattening regime. For $\gamma = 6.5$, the ellipsoid is a prolate spheroid whereas it is an oblate spheroid for $\gamma = k \times \gamma_{T,F}$, where $k$ is an integer. For comparison the shape variations of fabric ellipsoids in simple shear are also presented (Fig. 11).

When the ratio $\dot{\gamma}/T'_{22}$ is increased, the same general evolutions are observed except that: (a) the 'period' $\gamma_{T,F}$ decreases, approaching the asymptotic value $2\pi/(1 - K^2)^{1/2}$ (=8.8, for $K = -0.7$) of simple shear regime, and (b) the boundaries $\alpha_{min}$ and $\alpha_{max}$ approach $-45°$ and $+45°$, respectively.

*Influence of the shape coefficient* K—*case of heterogeneous populations*. The duration $\gamma_{T,F}$ of the one cycle of evolution decreases when the absolute value of $K$ approaches 0. Consequently for a given amount of strain, subfabric ellipsoids corresponding to various $K$ will have different orientations of their $\Lambda_1$ axes. So monoclinic fabrics are expected when the population is morphologically heterogeneous. The example of a simulated monoclinic pole-figure is presented in Fig. 12(a), with the corresponding $X'_1 - X'_3$ density profile (Fig. 12b). The tadpole-shaped pole-figure (Fig. 12a) is similar to the M4 fabrics of Fig. 1. The exact shape of the pole-figures depends on the strain regime, the amount of strain and the composition of the heterogeneous population of axial markers (Laporte 1987).

In Fig. 12(c), the asymmetric density profile of Fig. 12(b) is decomposed into symmetric profiles corresponding to the three homogeneous classes of markers. It appears that the density maximum of the tadpole-shaped fabric is defined by the highly anisometric markers ($K = -0.78$), markers with lower anisometry (mainly $K = -0.68$) composing the low density 'tail of the tadpole'. Consequently, as in the case of simple shear (Fig. 8b), the polarity of a tadpole-shaped fabric may be used to infer the sense of shear of the strain regime.

*Fabrics resulting from a polyphased strain history: example of a simple shear acting upon an axial flattening fabric*

Only the case of parallel flattening and shear planes is considered in the following (for the case of oblique flattening and shear planes, see Laporte 1987). For homogeneous populations of axial markers, the resulting fabrics are described by ellipsoids (Willis 1977, p.890). In a given direction $d$, the density of orientation $D_{2,d}$ produced by a simple shear acting upon an isotropic population is computed using Willis's model. Let $d'$ be the initial orientation—before simple shear—of an axial marker having the final orientation $d$; knowing $d$, $d'$ may be calculated using equation (6). Then the bulk density $D_d$ along $d$, resulting from the polyphased strain history, is given by the relation:

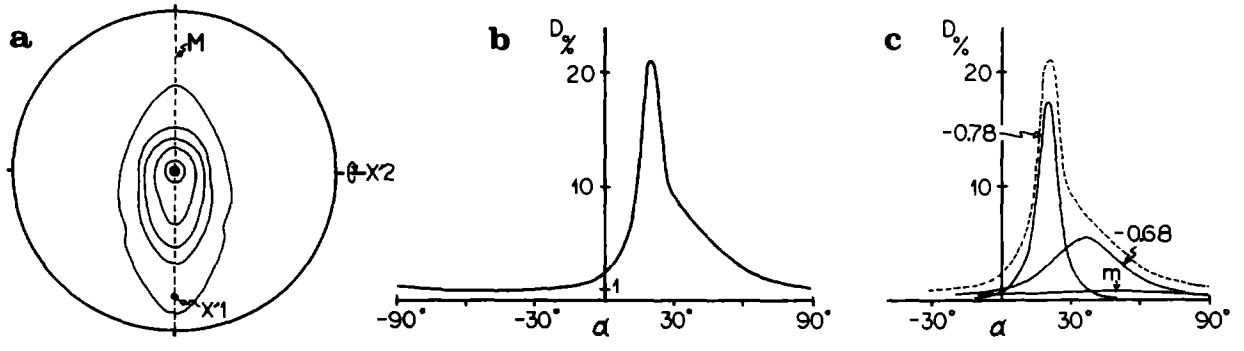


Fig. 12. Monoclinic fabric associated with non-coaxial flattening ($\gamma = 7.7$; the heterogeneous population is made of markers with $K = -0.58$, $-0.68$ and $-0.78$ in the respective proportions 0.25, 0.50 and 0.25); (a) tadpole-shaped pole-figure (contours: 1, 2, 3, 5 and 12%; maximum = 21%); (b) density profile $X'_1 - X'_3$ for the bulk fabric; (c) decomposition of the asymmetric profile (b) into its symmetric components (m gives the orientation of the density maximum for $K = -0.58$).

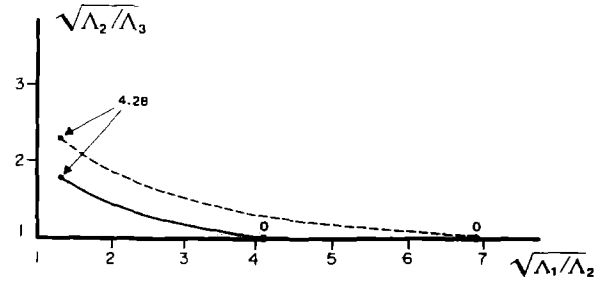


Fig. 13. Simple shear acting upon an axial flattening fabric: evolution of the shape of the fabric ellipsoid for shortening percentages of 75% (full line) and 85% (dashed line) during simple shear ($\gamma$ increasing from 0 to 4.28); axial markers with $K = -0.68$.

$$D_d = D_{2,d} \times D_{1,d'}, \tag{13}$$

where $D_{1,d'}$ is the density of orientation along $d'$, resulting from the first phase of axial flattening; $D_{1,d'}$ is computed from the equations describing the relationships between fabric ellipsoid and strain ellipsoid in coaxial strain regimes (Fernandez 1984). Below, the amount of axial flattening is specified by the shortening percentage $R$ in the $X_3'$ direction: for example, a shortening of 75% means that the final length along $X_3'$ is a quarter of the initial length. In order to draw pole-figures, the density $D_d$ is computed in a set of given directions. A more accurate knowledge of the fabric is gained by determining the value and the orientation of the principal axes of the fabric ellipsoid. The bulk symmetry of the strain history is monoclinic; the symmetry plane $X_1' - X_3'$ coincides with one of the symmetry planes of the fabric ellipsoid: so two of the principal axes may be determined by calculating the minimum and the maximum densities of the density profile $X_1' - X_3'$; the orientation of these two axes is computed with an accuracy of $\pm 1°$. The third principal axis of the fabric ellipsoid coincides with axis $X_2'$.

*Fabric development for homogeneous populations.* During simple shear, the shape of the fabric ellipsoid evolves as indicated in Fig. 13 for $K = -0.68$; this evolution depends strongly on the shortening percentage $R$ before simple shear (Fig. 13). Figures 14 and 15 show the variations in value and orientation of $\Lambda_1$ axis for shortening percentages of 75 and 85%. The curves $\Lambda_1 - \gamma$ and $\alpha - \gamma$ display the period $\gamma_{T,F} = 2\pi/(1 - K^2)^{1/2}$, already derived in simple shear regime; when $\gamma = \gamma_{T,F}$, the flattening fabric is restored. Two contrasting behaviours of $\Lambda_1$ (and consequently of the foliation $S$, parallel to $\Lambda_2 - \Lambda_3$) are shown in Fig. 15:

(i) *Behaviour* I: for high shortening percentages ($R = 85\%$), the foliation $S$ completes a full rotation around $X_2'$ when the amount of shear increases from 0 to $\gamma_{T,F}$; for $\gamma = \gamma_{T,F}/2$, $S$ is normal to the shear plane $X_1' - X_2'$.

(ii) *Behaviour* II: for lower shortening percentages ($R = 75\%$ or less; Laporte 1987), the variations of $\Lambda_1$ are restricted to a limited interval of the angle $\alpha$ ($-21° < \alpha < +21°$ for $R = 75\%$); for $\gamma = \gamma_{T,F}/2$, the angle $\alpha$ equals 0°: the foliation $S$ is parallel to the plane $X_1' - X_2'$.

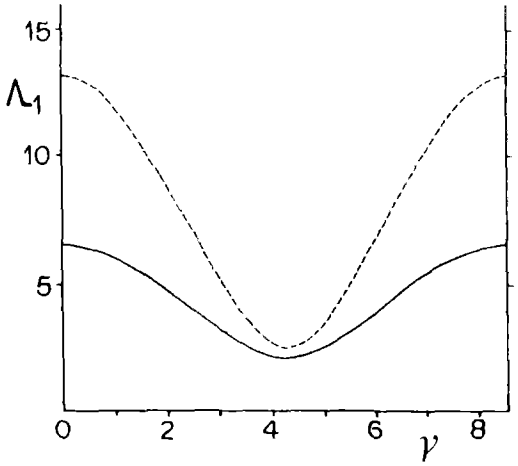


Fig. 14. Simple shear acting upon an axial flattening fabric: evolution of $\Lambda_1$ during simple shear for initial shortening percentages of 75% (full line) and 85% (dashed line).

The minimum value of axial flattening necessary for the fabric ellipsoid to display the first kind of behaviour has been computed for various shape coefficients $K$ (Fig. 16).

*Case of heterogeneous populations.* Two monoclinic fabrics related to polyphase strain histories are presented in Figs. 17 and 18 (for the same heterogeneous population (Table 2) and amount of shear ($\gamma = 3.2$)). In Fig. 17, the shortening percentage is 75%: the $X_1' - X_3'$ density profile shows a poorly-defined asymmetry. In Fig. 18 ($R = 85\%$), the $X_1' - X_3'$ density profile has a well-defined asymmetry and the pole-figure is very similar to the M4 diagram of Fig. 1. The origin of the discrepancies between Figs. 17 and 18 can be explained by referring to Fig. 16. For $R = 85\%$, subfabric ellipsoids with $K > -0.83$ are able to complete a full rotation around $X_2'$; thus, for a given amount of shear, ellipsoids

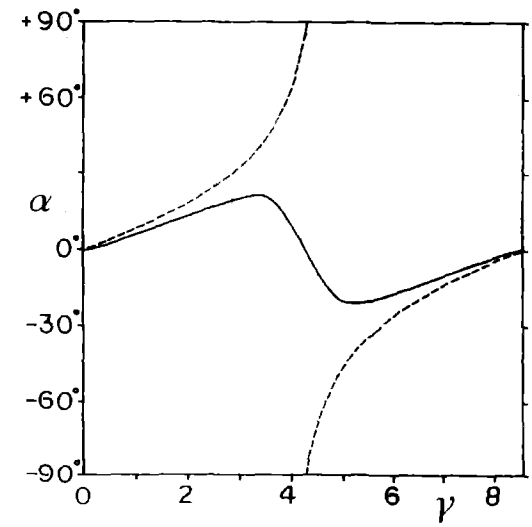


Fig. 15. Simple shear acting upon an axial flattening fabric: evolution of the orientation $\alpha$ of $\Lambda_1$ axis during simple shear for initial shortening percentages of 75% (full line) and 85% (dashed line).

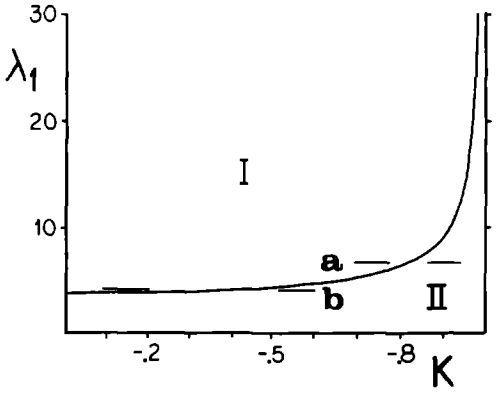


Fig. 16. Diagram $\lambda_1 - K$ delimiting the fields for the behaviours I and II of the $\Lambda_1$ axis of the fabric ellipsoid (see text for explanations). $\lambda_1$ is the long quadratic axis of the strain ellipsoid for the first phase of flattening. $\lambda_1 = 1/(1 - R)$; (a) $R = 85\%$; (b) $R = 75\%$.

corresponding to various $K$ values may have markedly different orientations (Table 2). For $R = 75\%$, fabric ellipsoids with $K$ less than about $-0.4$ plot in the field II of Fig. 16; accordingly, the $\Lambda_1$ axes of the subfabric ellipsoids are close to one another (Table 2) and the monoclinic symmetry of the bulk fabric is not distinct.

## DISCUSSION AND CONCLUSIONS

Models describing the behaviour of rigid markers suspended in a slowly deforming ductile matrix (Jeffery 1922, Willis 1977) have been used to specify the significance of various kinds of magmatic fabrics. As predicted by these models, the characteristics of P.D.O. are strongly dependent on: (a) the strain regime and the magnitude of the finite strain and (b) the shape of the markers (strictly the morphological composition of the population of markers). Several restrictive conditions of Jeffery's model have to be remembered: (a) the density contrast between the rigid marker and its matrix is negligible; (b) the marker is ellipsoidal and its shape does not evolve during motion; (c) the ellipsoid is isolated: it does not interact with neighbouring grains; and (d) the deforming fluid has a Newtonian behaviour (Willis's model has a somewhat broader field of application particularly because it may be extended to more general ductile behaviour; however the useful notion of fabric ellipsoid is restricted to axially symmetric markers). Obviously premises (a)–(c) are never strictly realized in natural conditions. For instance interactions between neighbouring grains are expected when the crystal content of the deforming magma is high. Consequently quantitative informations which might result from the statistical analysis of natural fabrics, have to be considered with caution. However the qualitative results, particularly the relationships between fabric shape and strain regime geometry, remain valid even though the restrictive conditions of the theoretical models may not be fully satisfied.

Jeffery's and Willis's models associated with Curie's Principle lead to the following conclusions.

(i) Low symmetry fabrics result from non-coaxial strain regimes. More precisely, monoclinic fabrics are associated with monoclinic non-coaxial strain regimes such as simple shear. Triclinic fabrics are predicted to result from non-coaxial strain regimes with triclinic symmetry.

(ii) High symmetry fabrics may result from coaxial as well as non-coaxial strain regimes. Indeed, the latter lead to highly symmetric fabrics when they act upon homogeneous populations of axial markers (Willis 1977). However, morphological homogeneity and axisymmetry of the markers are not realistic assumptions so that natural fabrics resulting from non-coaxial strain regimes should commonly have a low symmetry. Unfortunately, the corresponding pole-figures may have a poorly-defined asymmetry (e.g. Fig. 17), making them difficult to discriminate from high symmetry diagrams. Consequently a detailed scrutiny of natural pole-figures is required and the principles we outlined should not be applied to fabrics with an ill-defined symmetry.

(iii) Monoclinic fabrics contain precious information about the deformation they result from: (a) the plane $X'_1 - X'_3$ of the non-coaxial strain regime (Figs. 2c & d) coincides with the symmetry plane of the monoclinic pole-figure; (b) the sense of shear may be inferred from the polarity of the pole-figure as illustrated in Fig. 8(b) (complements and limitations to this criterion are given

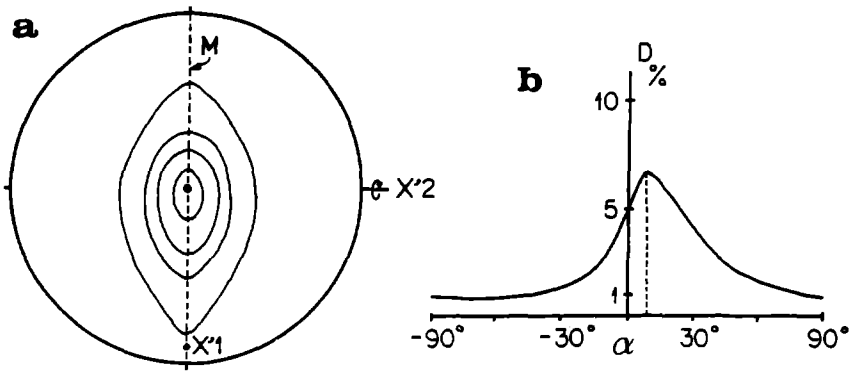


Fig. 17. Monoclinic fabric with poorly-defined asymmetry associated with a polyphased strain history: axial flattening ($R = 75\%$) followed by simple shear ($\gamma = 3.2$); the heterogeneous population of axial markers is defined in Table 2. (a) Pole-figure with contours 1, 2, 3 and 5%; maximum = 6.7%. (b) Density profile $X'_1 - X'_3$.

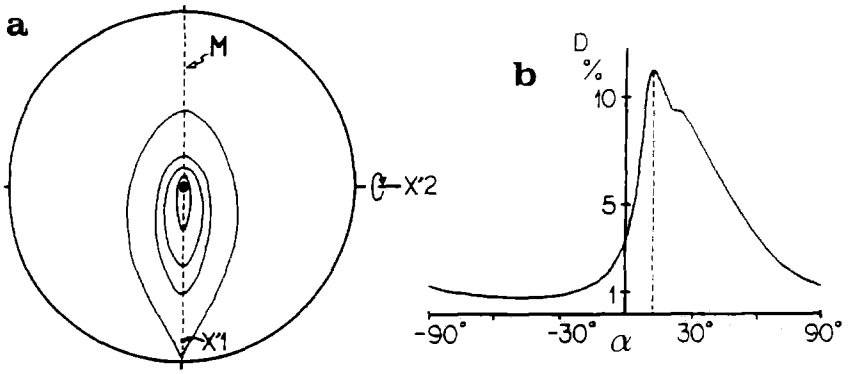


Fig. 18. Monoclinic fabric with well-defined asymmetry; same conditions as for Fig. 17 except the initial shortening percentage $R = 85\%$. (a) Pole-figure with contours 1, 3, 5 and 8%; maximum = 11.3%. (b) Density profile $X'_1 - X'_3$.

above); and (c) various types of non-coaxial strain regimes or strain histories may be distinguished by the geometrical characteristics of the preferred orientations they produce. This was established above by comparing M1 and M4 monoclinic fabrics (Fig. 1): M1 fabrics are associated with simple shear whereas the development of M4 fabrics involves the combination (or the succession) of a coaxial deformation and a simple shear.

Finally, quantitative information may be drawn from the statistical analysis of magmatic fabrics. For instance, P.D.O. defined by K-feldspar megacrysts have been used to quantify the strain recorded in porphyroid granitoids (Fernandez & Laboue 1983, Fernandez 1984, Laporte 1987). Once the geometry of the strain regime has been inferred from the characteristics of the resulting fabric, the magnitude of the finite strain may theoretically be estimated knowing the shape of the markers. In simple shear regime, the amount of shear may be deduced from: (a) the value of the density maximum of the fabric; (b) the angular mismatch between two subfabrics, measured in the symmetry plane $X'_1 - X'_3$ of the strain regime (Figs. 6 and 8a); and (c) the angle between the foliation plane of the fabric and the shear plane when the orientation of the latter is known (see Fig. 6 and Blanchard *et al.* 1979).

For general non-coaxial strain regimes, it is not possible to get a full quantitative description of the strain from a resulting fabric. A major hindrance is that the same pattern of P.D.O. may be associated with different strain regimes or histories (see above the case of M4 monoclinic pole-figures). Consequently, external constraints are first required to select the right model. For instance, M4 pole-figures of the Ile-Rousse pluton, northwestern Corsica, have been ascribed to a polyphased history involving the succession flattening/simple shear (Laporte 1987). This conclusion was based on the following information: (a) the existence of flattening fabrics with axial symmetry, in addition to M4 monoclinic fabrics; (b) the structural symmetry at the scale of the pluton; and (c) the pancake shape of the basic microgranular enclaves in the granitoids. According to our calculations, the development of Ile-Rousse M4 fabrics required shortening in excess of 75% and shears up to 4 or 5. Consistently, shortenings estimated from the axial fabrics and the oblate enclaves locally exceed 75%.

As illustrated by the example of Ile-Rousse pluton, it may be concluded that, combined with other structural approaches, statistical analysis leads to qualitative as well as quantitative information on the deformations responsible for the development of magmatic fabrics. Such information is required to decipher the complex history of emplacement and deformation of igneous bodies.

Table 2. Orientation of the $\Lambda_1$ axis of the subfabric ellipsoids for the bulk fabric displayed in Fig. 17 (column $\alpha_1$, $R = 75\%$, $\gamma = 3.2$) and in Fig. 18 (column $\alpha_2$, $R = 85\%$, $\gamma = 3.2$); the columns $K$ and % define the composition of the population of rigid markers

| $K$ | % | $\alpha_1$ (°) | $\alpha_2$ (°) |
|---|---|---|---|
| −0.48 | 10 | 32 | 65 |
| −0.58 | 20 | 27 | 51 |
| −0.68 | 40 | 21 | 37 |
| −0.78 | 20 | 14 | 24 |
| −0.88 | 10 | 6 | 11 |

## REFERENCES

Blanchard, J.Ph., Boyer, P. & Gagny, C. 1979. Un nouveau critère de sens de mise en place dans une caisse filonienne: le "pincement" des minéraux aux épontes. *Tectonophysics* **53**, 1–25.

Blumenfeld, P. & Bouchez, J.-L. 1988. Shear criteria in granite and migmatite deformed in the magmatic and solid states. *J. Struct. Geol.* **10**, 361–372.

Curie, P. 1894. Sur la symétrie dans les phénomènes physiques, symètrie d'un champ électrique et symétrie d'un champ magnétique. *J. Phys., Paris* **3**, 393–415.

Debat, P., Sirieys, P., Deramond, J. & Soula, J. C. 1975. Paleodéformations d'un massif orthogneissique (massif des Cammazes, Montagne Noire Occidentale, France). *Tectonophysics* **28**, 159–183.

Fernandez, A. 1982. Significiation des symétries de fabrique monocliniques dans les roches magmatiques. *C.r. Acad. Sci., Paris* **294**, 995–998.

Fernandez, A. 1984. Etude théorique et expérimentale du développement de la fabrique dans les roches magmatiques. Application à l'étude structurale des granitoïdes. Unpublished Thèse Etat, University of Clermont Ferrand II.

Fernandez, A., Feybesse, J. L. & Mezure, J. F. 1983. Theoretical and experimental study of fabrics developed by different shaped markers in two-dimensional simple shear. *Bull. Soc. geol. Fr.* **25**, 319–326.

Fernandez, A. & Laboue, M. 1983. Développement de l'orientation préferentielle de marqueurs rigides lors d'une déformation par aplatissement de révolution. Etude théorique et application aux

structures de mise en place du granite de la Margeride au voisinage du bassin de Malzieu. *Bull. Soc. geol. Fr.* **25**, 327–334.

Flinn, D. 1962. On folding during three-dimensional progressive deformation. *Q. Jl geol. Soc. Lond.* **118**, 385–433.

Freeman, B. 1985. The motion of rigid ellipsoidal particles in slow flows. *Tectonophysics* **113**, 163–183.

Gay, N. C. 1968. The motion of rigid particles embedded in a viscous fluid during pure shear deformation of the fluid. *Tectonophysics* **5**, 81–88.

Jeffery, G. B. 1922. The motion of ellipsoidal particles immersed in a viscous fluid. *Proc. R. Soc. Lond.* **102A**, 161–179.

Laporte, D. 1987. Un exemple d'intrusion syntectonique: l'intrusion d'Ile-Rousse, Corse du Nord-Ouest. Etude pétrographique, minéralogique et géochimique. Analyse structurale. Unpublished thèse, University of Saint-Etienne.

Nicolle, J. 1950. *La Symétrie et ses Applications*. Michel, Paris.

Paterson, M. S. & Weiss, L. E. 1961. Symmetry concepts in the structural analysis of deformed rocks. *Bull. geol. Soc. Am.* **72**, 841–882.

Ramberg, H. 1975. Particle paths, displacement and progressive strain applicable to rocks. *Tectonophysics* **28**, 1–37.

Reed, L. J. & Tryggvason, E. 1974. Preferred orientation of rigid particles in a viscous matrix deformed by pure shear and simple shear. *Tectonophysics* **24**, 85–98.

Sander, B. 1948. *Einführung in die Gefügekunde der geologischen Körper*. Springer, Vienna.

Tullis, T. E. 1976. Experiments on the origin of slaty cleavage and schistosity. *Bull. geol. Soc. Am.* **87**, 745–753.

Weiss, L. E. & Wenk, H.-R. 1985. Symmetry of pole figures and textures. In: *Preferred Orientation in Deformed Metals and Rocks. An Introduction to Modern Texture Analysis* (edited by Wenk, H.-R.). Academic Press, Orlando, Florida, 1–10.

Willis, D. G. 1977. A kinematic model of preferred orientation. *Bull. geol. Soc. Am.* **88**, 883–894.